Open access • Journal Article • DOI:10.1016/J.SNB.2018.12.030

Chronic neural recording with probes of subcellular cross-section using 0.06 mm² dissolving microneedles as insertion device — Source link

Frederik Ceyssens, Marta Bovet Carmona, Dries Kil, Marjolijn Deprez ...+6 more authors

Institutions: Katholieke Universiteit Leuven, Université catholique de Louvain

Published on: 01 Apr 2019 - Sensors and Actuators B-chemical (Elsevier)

Topics: Electrode array

Chronic neural recording with probes of subcellular cross-section using 0.06 mm^2 dissolving microneedles as insertion device

Frederik Ceyssens[1], Marta Bovet Carmona[2], Dries Kil[1], Marjolijn Deprez[3], Ester Tooten[4], Bart Nuttin[3], Aya Takeoka[5], Detlef Balschun[2], Michael Kraft[1], Robert Puers[1]*

[1]ESAT-MICAS, KU Leuven, Kasteelpark Arenberg 10, 3001 Leuven, Belgium.
[2] Laboratory for Biological Psychology, Brain & Cognition, KU Leuven, Tiensestraat 102, 3000 Leuven, Belgium.

[3]Experimental Neurosurgery and Neuroanatomy, UZ Herestraat 49 box 7003, 3000 Leuven, Belgium.
[4]Université Catholique de Louvain, WinFab, Place du Levant 3, 1348 Louvain-la-Neuve, Belgium.
[5] Neuro-Electronics Research Flanders (NERF), Kapeldreef 75, 3001 Leuven, Belgium.

**Corresponding author. fceyssen@esat.kuleuven.be - Tel. 0032 16 321093*

E-mail addresses: fceyssen@esat.kuleuven.be, marta.bovetcarmona@kuleuven.be, dkil@esat.kuleuven.be, marjolijn.deprez@kuleuven.be, ester.tooten@uclouvain.be, bart.nuttin@kuleuven.be, Aya.Takeoka@nerf.be, detlef.balschun@kuleuven.be, Michael.kraft@esat.kuleuven.be, robert.puers@esat.kuleuven.be

Keywords: chronic neural recording; ultra-flexible; biodegradable; dissolvable; resorbable; microneedles

Abstract

Ultra-flexible electrode arrays with a cross-sectional area of only a few µm² show great promise for long-term, high resolution neural interfacing without detrimental scar tissue formation. However, due to their low stiffness, insertion is a challenge. In this work, we investigate microneedles consisting of quickly biodegradable, short-chained, acid terminated PLGA (50:50 lactide:glycolide ratio) as insertion device for a polyimide-based neural electrode array of 1 µm thickness. An upscalable, wafer-level fabrication process is presented. Both separate PLGA microneedles as well as complete, assembled neural probes were tested in vivo for up to 4 months. The arrays allowed to record spontaneous spike activity and evoked local field potentials in the somatosensory cortex of rats on all measured timepoints. Very limited lesion formation, measuring about 20% of the cross sectional area of the original microneedle, was observed. Neurons can be seen to infiltrate the area originally taken up by the dissolving PLGA microneedle. The results indicate that the presented electrode arrays and insertion method are well suitable for application in long-term, high resolution neural recording.

1. Introduction

Currently, a significant research effort towards high-resolution neural interfaces is going on worldwide. Drastically increasing the channel count will yield an enormous leap forward fundamental neuroscientific research of cognition and disease [1], will allow the development of more advanced sensory and motor prostheses [2], and could eventually allow humans to interface seamlessly with machines by thought alone [3].

We can state that the ideal neural interfacing device lasts for a lifetime, does not disturb the existing neural networks, and yet is able to interact with a vast population of individual neurons in a large brain volume.

Currently, the most advanced systems in terms of channel count are active needle-shaped electrode arrays, fabricated by lithographic postprocessing of silicon wafers that already contain CMOS electronics [4]. The most advanced development of such implants contains 1356 electrodes of which 678 can be monitored in parallel [5]. However, the long-term performance of such implants is not satisfying. Commonly, after a few months, the quality and number of active channels drops and post mortem scar tissue formation around the implant is observed [6]. The body's inflammatory response is even able to corrode silicon [7] and dissolve silicon oxide passivation layers [8] over a period of months.

The cause of the inflammatory reaction has been attributed to the mismatch in compliance between the relatively stiff implant and the surrounding brain tissue [9], which has a Young's modulus of just a few kPa [10]. As even in anaesthetized animals the brain tends to pulsate with amplitudes of 10-30 µm driven by the irregularities in blood flow [11], there will be a constant source of irritation present even after the initial trauma of the implantation period has been resolved. This, provokes a chronic inflammatory response [12]. Mechanically more compliant implants were shown to yield a reduced inflammatory response compared to similar, less compliant devices [13]. Considering the issues raised above, several researchers focused on the use of stable, low Young's modulus polymeric materials [14, 15] and, as compliance is proportional to the third power of the diameter, on reducing implant cross-section [16, 17].

Recently, in a further evolution of this concept, mesh or ribbon shaped implants with cross sections in the order about 10 µm², i.e. smaller than a single cell, have been demonstrated. Researchers have proven that such polymer-insulated, ultra-thin neural implants can be placed in the brain over chronic timescales of up to one year without the formation of scar tissue [18]. To achieve implantation of these devices that are too compliant for insertion as such, they were suspended in saline water and injected using a capillary. Only then, during surgery, the array was attached to a connector and electronics using conductive ink. Another recent work successful in this aspect used a Focused Ion Beam (FIB) machined pin-like insertion device [19] to place ribbon-shaped electrode arrays in the brain. Yet another interesting approach – only demonstrated in vitro so far - is the use of a stylet-shaped insertion device disattached after insertion by dissolution of a magnesium sacrificial layer [20].

To achieve high channel count recording with thin polymer electrode arrays distributed over an extended brain volume, a large number of electrodes would need to be inserted. Unfortunately, the aforementioned approaches require a relatively cumbersome implantation procedure which makes them difficult to scale up to higher electrode and needle shaft counts.

A more straightforward approach would be to embed the ultra-thin electrode array in a needle or needle array that dissolves after implantation. Several authors have published about the use of materials such as ice [21], carboxy-methylcellulose (CMC) [22], gelatin [23], silk [24, 25], polyethylene glycol (PEG) [24], maltose [26] and tyrosine-derived terpolymers [27] to temporarily reinforce neural implants.

Conceptually easy as this might be, such embedding methods are hard to implement on ultrathin electrode arrays that are too frail to be handled without support. The publications cited above typically use dip coating, which requires the arrays to be released from the substrate on which they were fabricated first, before the dip coating step. As at this point they are no longer mechanically

supported, they inherently require some remaining mechanical stiffness. The rapid water solubility of the materials reported so far precludes the use of all common sacrificial layers that would allow removing the assembly from the carrier wafer after embedding. Hence, thicker (>10 µm) electrode arrays, or rolling up of ultra-thin arrays, are required. This could be one reason why so far these methods have not been able to reach the same level of seamless neural tissue integration as has been shown possible with micrometer-thin implants.

A second point of concern is the fact that most of the materials used so far dissolve or soften so quickly that rapid insertion is needed, impeding handling and positional correction. In the case of carboxy-methylcellulose, significant swelling was reported as well [22].

In this paper, we address these issues by using short-chained, acid-terminated PLGA (polylactic-co-glycolic acid) microneedles as the temporary carrier for ultra-thin electrode arrays. We will show that it is possible to embed a 1 µm thick neural electrode array in these microneedles. Then, their long-term in vivo performance for neural recording is assessed in a proof-of-concept test over a period of 4 months.

2. Materials and Methods

2.1 Introduction

In this section, a brief overview is given of the materials and methods used. For an in-depth description, the reader is referred to the supplementary section “Detailed Methods”.

2.2 Selection of resorbable material

The dissolution time of the temporary reinforcement needs to be lower than 4 weeks, as experiments indicate permanent scar formation by needle-shaped objects that remain in the brain for a longer period [29]. Still, the material has to be compatible with a sacrificial layer release step, required to dislodge the fine electrode structures from their carrier wafer. The latter precludes most materials used so far to fabricate temporary needle structures, as they quickly dissolve in water. More classic resorbable polymer materials such as polycaprolactone, polyglycolic acid (PGA) and polylactic acid (PLA) were ruled out as they typically degrade with a half-life of one or more months [30].

PLGA, more specifically acid-terminated poly (D,L-lactide co-glycolide) in which the lactic and glycolic acid groups are present in a 1:1 ratio is an exception to this. It has a half life as short as one week [30]. The material is commercially available under the name Corbion Purasorb PLDG 5002A, and is approved for human use. To the best of our knowledge, this material has not been tested before to insert thin film neural implants.

As the degradation products of the material are acids, we suspected that the degradation reaction would be slowed down in an acidic environment as per Le Chatelier’s principle. This was confirmed in a soak test in 5% HCl. Small micromolded objects immersed for 3 days did not show any visible degradation, which makes the material highly compatible with the sacrificial layer release step used in our fabrication process. Reversely, the same objects degraded quickly when put in an alkaline

environment. Considering the above, Corbion Purasorb PLDG 5002A was selected for use in this work.

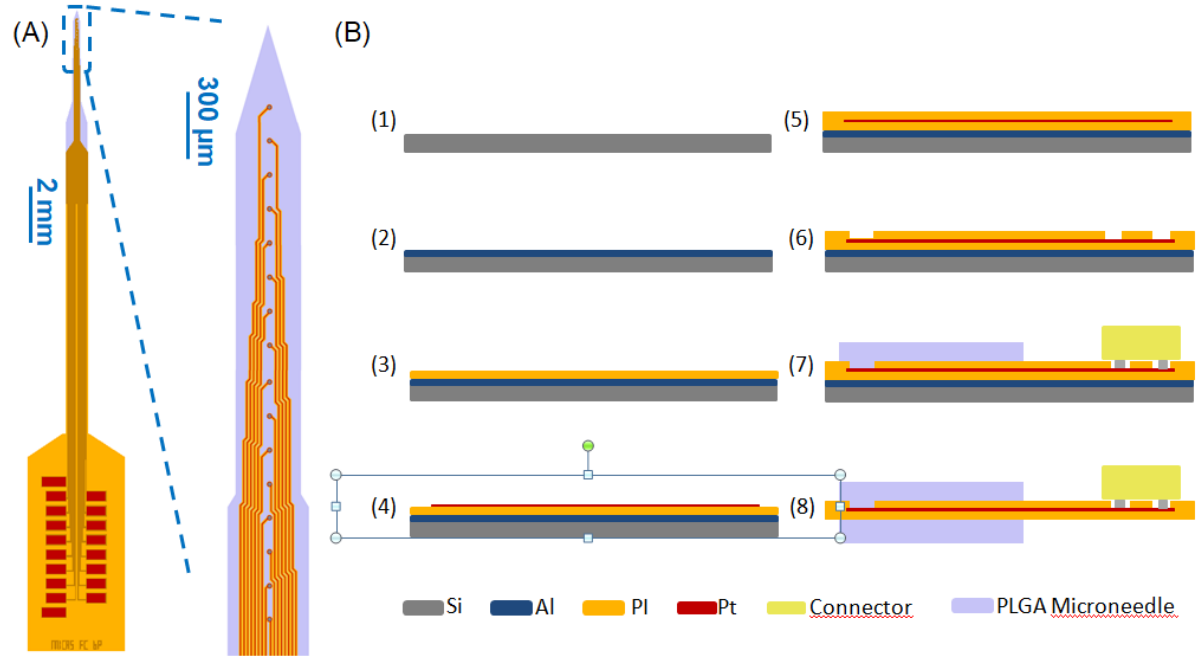

Fig. 1: (A) Design of implant. (B) Fabrication procedure: (1) Si substrate (2) sacrificial layer (3) PI (4) patterned Pt & Irox (5) second PI (6) patterning PI (7) bonding connector and microneedle (8) release from substrate, bonding second microneedle.

2.3 Electrode array design

The wafer-level design requires only two masks. Arrays containing 16 electrodes of 18 µm diameter were designed (Fig. 1A). The designed insertion depth is 2.5 mm, spanning all layers in a rat cerebral cortex. The electrodes are arranged in a linear fashion, 150 µm apart. The designed width of the metal tracks between the electrodes and the connector is 3 µm and there is 5 µm of insulation on the left and right side. In the part that will penetrate the brain, the individual metal tracks are not mechanically interconnected by the insulation layer, insuring maximum flexibility. On the other side of the device, bondpads are foreseen matching the footprint of a 18-pins Omnetics Nano connector.

2.4 Fabrication

We fabricated the non-resorbable electrode array backbone using a process optimized for extended insulation lifetime [31]. The electrode arrays consist out of polyimide (PI), iridium and platinum, already shown to be highly biocompatible [32, 33, 34]. We adapted the fabrication process to reduce the total array thickness to 1 µm. Sputtered iridium oxide was used as electrode material to reduce impedance [35].

Microneedles were fabricated using picosecond pulsed UV laser machining out of PLGA sheets. The electrode arrays backbone was then thermally bonded between two 100 µm thick PLGA microneedles. This is necessary as preliminary insertion tests in 0.6% agar gel, a realistic mock brain

model used for mechanical testing [36], showed detachment of the fine wires and electrodes if a single 200 µm thick microneedle was used.

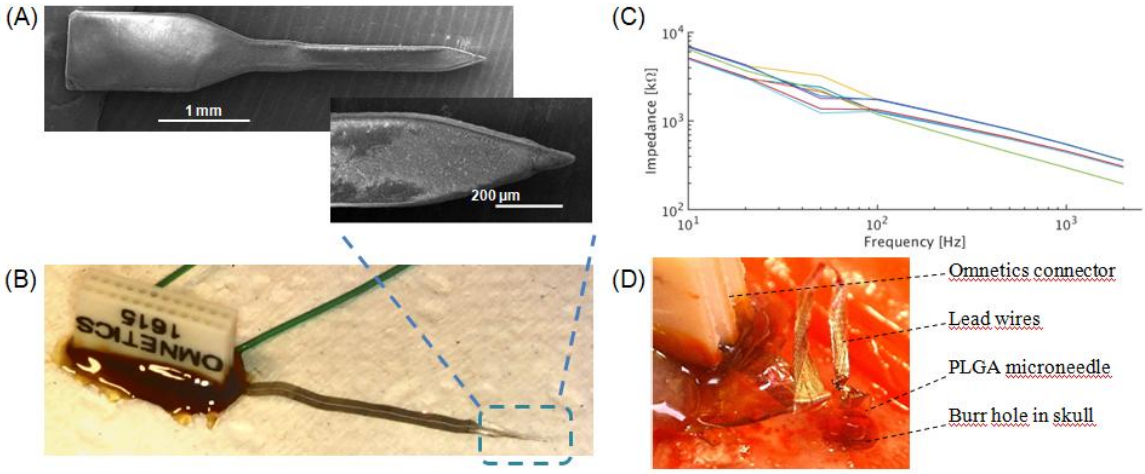

Fig.2.(A) PLGA microneedle fabricated my laser machining. (B) Assembly of Omnetics connector, ultra-fine electrode array and PLGA microneedle. (C) Measured impedance spectrum in PBS. (D) picture taken during implantation.

2.5 In vivo tests

To characterize the chronic neural recording capabilities of the electrode arrays, they were implanted in the sensorimotor cortex of four rats and used to record spontaneous spikes and evoked local field potentials in sessions spread out over the course of 4 months. The rats were anesthetized during the tests and housed in an animal facility under normal conditions in between. Electrical forepaw stimulation was applied and the peak-to-peak (PTP) values of the evoked potential in the brain were determined, as well as its root mean square (RMS) value. Also, spontaneous firing of action potentials was monitored in a 4 minute period during which no stimulation was applied. Spikes were counted using a open source peak detection algorithm [28]. The impedance of the electrodes with respect to a reference electrode situated in the skull was also determined before, 2 and 4 months after implantation at a frequency of 1004 Hz.

At the end of the experiment, the animals were perfused and slices were made of the relevant section of the brains. The slices were stained using immunohistological methods: NeuN staining for viable neural nuclei and GFAP for detecting astrocyte scar formation. The area of the remaining scar was determined, as well as the neuron density in and between circles of 300, 600 and 1000 µm diameter around the implant. Before the aforementioned experiment a pilot test was conducted in which only PLGA needles without the electrodes were implanted, for which the same perfusion and histology protocol was used.

3. Results

3.1 Fabrication

The fabrication of the electrode arrays went as planned. The yield of the process was about 80% and the accuracy of linewidths and electrode diameters was within 2 µm. A fabricated PLGA microneedle can be seen in Fig. 2A. With a measured tip radius of about 15 µm, the laser fabricated needles are of sufficient sharpness to penetrate the brain after opening the dura mater as became clear during later experimentation. The laser cutting accuracy was within 10 µm.

A completed assembly of an electrode array, an Omnetics connector and a PLGA microneedle can be seen on Fig. 2B. That figure also shows the green reference and ground wires attached to the connector. Fig. 2C shows the measured impedance spectrum of single electrodes versus a large Pt reference electrode in PBS. The values, on average 300 kΩ at 1 kHz, are acceptable for action potential recording. The standard deviation of the impedances is a factor of 4 higher compared to the pre-implant situation.

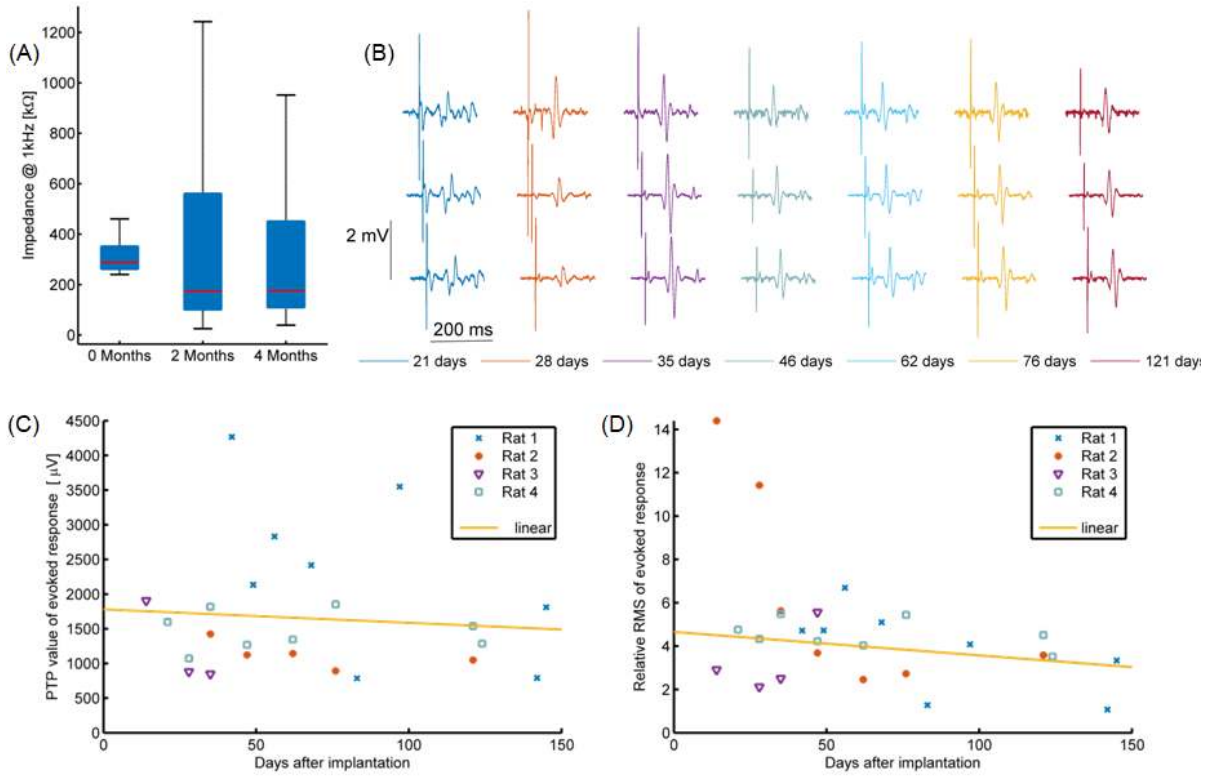

Fig. 3. (A) Boxplot of measured electrode impedances at 1 kHz before implantation, after 2 months of implantation and at the end of the experiment. The box is drawn between the 25th and 75th percentile and the red line denotes the median. (B) Representative excerpt from EP recordings from an electrode in a top, central and bottom position (in the same order in the figure). (C) Measured PTP values of evoked potentials as a function of time. (D) Measured RMS values of the EPs, relative to the pre-stimulus period.

3.2 Electrical measurements

The surgeries (Fig. 2D) and the rest of the animal study went as planned, with the exception that after 1 month one animal (rat 3) lost its headstage, so no more electrical measurements were possible.

The electrical measurement results are summarized in Fig. 3 and 4 for evoked and action potentials, respectively. Fig. 3A also shows the electrode impedance measurements before (in 0.9% NaCl), in the middle (2 months) and at the end of the experiment (4 months). The average values are shown to be relatively constant throughout the experiment. Although the variability increased after implantation, since the measured channel impedance was never larger than 1.2 MΩ recording was not hampered.

Evoked potentials (EPs) caused by forepaw electrical stimulation could be recorded consistently throughout the experiment on all channels. Figure 3B shows a representative sample from the EP recordings on rat 4. The first measured EP of each stimulation experiment is plotted for the bottom, center and top electrode. It can be seen that the presence and shape of the EP is quite consistent, though – with a few positive outliers - there is a variability of about 50% in size of both the stimulation artifact as well as the evoked response. Between channels, the EPs generally do not show much difference.

An overview of all the average PTP and RMS value of all EPs per rat and for every measured timepoint is given in Fig. 3C and 3D. It is shown that the evoked potentials are always clearly present, with PTP values between 0.8 mV and 1.9 mV. In rats 1 and 2, the average PTP values of the EPs were above that range in the first 1-2 months of the experiment, returning to values in line with the rest later. Linear interpolation reveals a slightly downward trend in signal amplitude, but considering the larger variability this is not statistically significant.

Spontaneous action potentials (APs) were also recorded at all time points of the experiment, on all electrodes. A small representative excerpt from the measurements (4 electrodes, 7 timepoints) can be seen in Fig. 4A. The figure shows an increase of AP frequency over time. From 46 days on, APs are more frequently present also in more superficial electrodes. Indeed, a plot of the total amount of APs observed per rat and per timepoint (Fig. 4B) reveals that 3 out of 4 rats went through an initial period (< 50 days) in which relatively little AP activity could be recorded, compared to later timepoints (> 50 days). More specifically, the frequency of occurrence of the action potentials was in the range of a few Hz in the first month, to stabilize later to a range of 10-90 Hz after about two months.

The average amplitude of the APs measured in each experiment (Fig. 4C) was stable, ranging between 90 and 150 µV in between experiments. In two rats (Rat 3 & 4), the average AP was considerably higher in strength, about 250 µV, in the first few weeks after implantation.

3.3 Histology

The histological results are summarized in Fig. 5. Neurons can be seen to have penetrated the area first occupied by the dissolving microneedle, both in case of bare PLGA needles (Fig. 5A) as well as when the needles carried an electrode array (Fig.5B). The area taken up by the scar and the area without neurons are plotted in Fig. 5C and compared to the area of the implant. The area of the scar as determined by on the GFAP stained slices, was only 11% of the original 0.06 mm^2 cross sectional area of the needle.

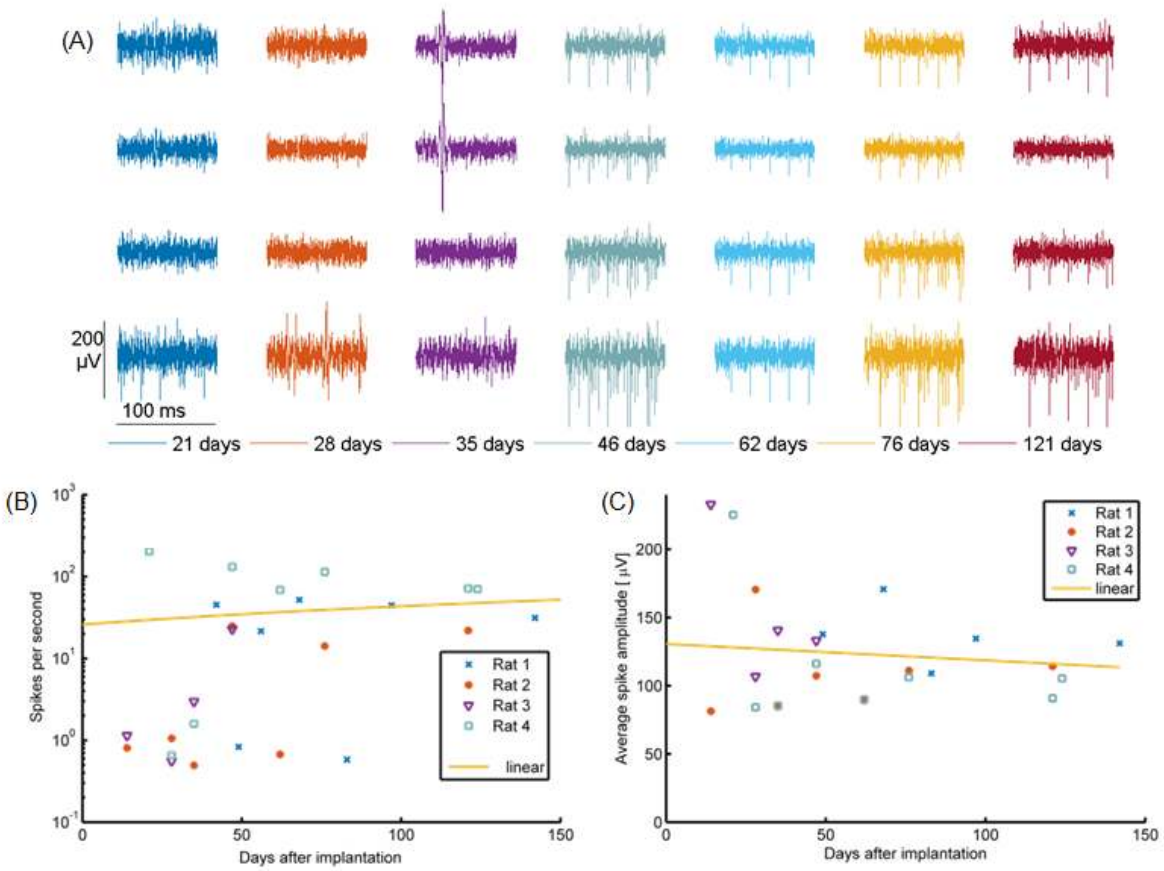

Fig. 4. (A) Small sample from recorded spontaneous action potentials (spikes) at different timepoints. Recordings of four electrodes shown, from top to bottom as placed in the brain. (B) Number of recorded spontaneous spikes per second for every rat and every timepoint tested. (C) Average spike amplitude of the action potentials over time in the same experiments.

The experiment in which the electrode array was added to the microneedle yielded similar results as can be seen on Fig. 5B. On these images, the electrode array itself is not visible as it was pulled out of the brain during when it was removed from the skull. The animals investigated showed a scar that was 20% in size compared to the cross sectional area of the PLGA microneedle (Fig.5D). We also counted the viable neurons on the NeuN stained slices as discussed in the methods section and did not observe a significant decline in neuron density when approaching the implant (Fig. 5E).

4 Discussion

This research was undertaken to develop a chronic neural interface, upscalable to high channel counts and practical in use. The results obtained show that the approach presented here is viable and deserves further study.

The non-resorbable, ultra-thin backbone of the device performed well in the in vivo experiments: no crosstalk was observed, indicating sufficient performance of the PI insulation layer. Furthermore, the

impedance of the iridium oxide electrodes remained stable and action potentials could be recorded in all timepoints. This contrasts well with earlier work on silicon probes, in which channel loss over time is frequent [6]. In [37] histology is performed on the neural tissue around a silicon needle of a size similar to the scar here after 4 months. However, 20% neural loss was reported, more than in this work.

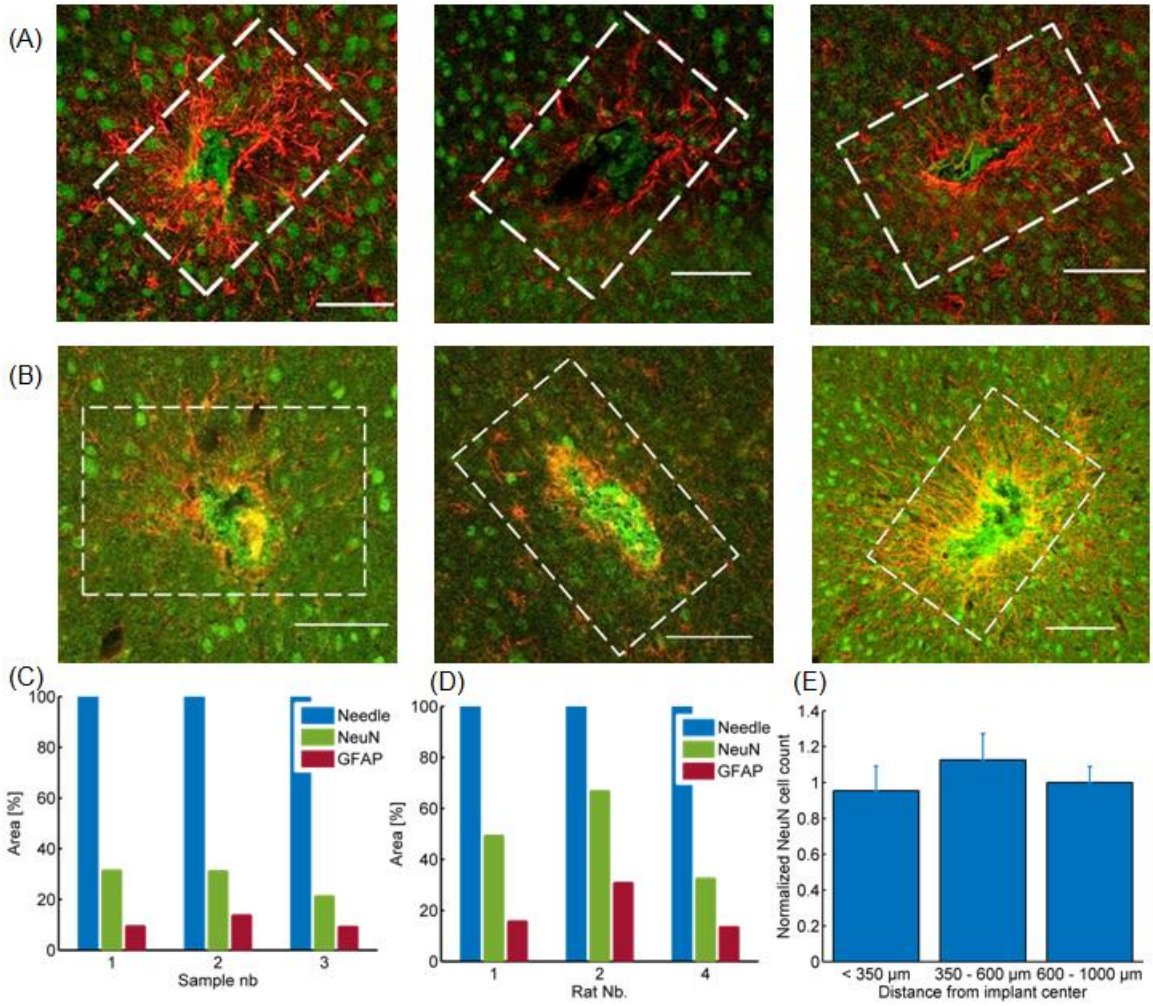

Fig.5. (A) GFAP / NeuN stained slices from the 3 implants of the pilot study that used PLGA microneedles not containing an electrode array. Contours of the original implanted needle are marked. Scale bar = 100 µm. (B) same for rat 1, 2 and 4 implanted with PLGA microneedles with electrode array. (C) cross sectional area of microneedle compared to lesion size in pilot study. (D) same for study PLGA microneedles with electrode array. (E) average neuron density in concentric circles around implant site, normalized to the outer circle.

In contrast to the very short dissolution times of the carrier material used in the cited literature, the PLGA microneedle chosen as temporary carrier needs several weeks to dissolve which allows for a straightforward fabrication procedure and reduces the complexity of the implantation. The remaining scar is minimal, only 20% of the size of the temporary carrier. We do not expect much extra scarring due to the longer dissolution time, as it is still below the Turner limit [29] of four weeks. Moreover, Kozai et al. showed that a dummy microneedle of very similar dimensions made from a much faster dissolving material caused comparable tissue damage [22].

What does seem to be related to the longer dissolution time is the period in which there is reduced action potential activity measured around the implant. This is inherent to the design, though it could be improved by ameliorating adhesion, allowing the electrodes to be positioned on the outside of the microneedles. For applications in for example advanced prostheses, the waiting time seems acceptable. For research applications the waiting time is definitely a disadvantage.

There was considerable variation in the electrical measurements, especially in the amount of APs recorded but also in terms of signal levels. Part of these variations, especially at the early timeponts, will be due to the changing environment in close vicinity to the electrode array and possible slight relative movement of the electrodes. The in vivo experimental setup in general will have contributed as well: the exact positioning of the stimulation electrode in the forepaw, the varying depth of isoflurane anesthesia depending on the weight gain of the rats during the experiment and natural individual variations will also have had their effect. In case of the measured evoked local field potentials, it must also be added that they originate from many, often distant sources [38] which are not necessarily affected by the implant. For our set purpose, to show the ability to record action potentials over chronic timespans, the in vivo experiment was adequate. However, in future work it could be interesting to be able to reduce experimental variation. Moreover, it would be interesting to investigate if the electrodes are suitable for stable single-neuron tracking. Studying the AP waveform changes with much shorter time intervals, or adding calcium imaging to the setup could answer the question if always the same neurons are being measured [39].

We have found only two other publications in which ultra-thin electrode arrays were combined with a dissolving insertion device. In [21], an electrode mesh was rolled up, wetted and frozen. This creates a cone of about 250 µm in diameter, featuring electrodes on the outside. Histology showed no void at the implant site after 5 weeks. There was evidence of cellular processes penetrating the mesh, though no neuron bodies did so. In [40], CMC microneedles were combined with thin Parylene-C coated electrodes, but no histological data or long term tests were shown.

In [22], nonfunctional CMC microneedles with a cross section of 300 x 125 µm² were compared with 100x125 µm² microneedles. The large version yielded similar histological results as our own work, while the small version yielded almost no signs of scarring and no central void.

This shows the most straightforward path to improve the concept presented: a further reduction of the implant's insertion vehicle size could impede scar tissue formation completely while leaving only very minimal implants in the brain. In contrast, further reduction of the cross-section is not likely to occur for high density silicon probes, hampered by mechanical issues such as the brittleness. Another approach which is upscalable to large electrode counts is the use of larger, polymer based implants that do not need an insertion aid [41][42]. Their long-term performance is not clear from literature at this point, but their inherent large cross-section will most likely put a lower limit on the obtainable tissue damage as a quantitative comparison between [41] and [22] already indicates.

In the presented work, size reduction will not be not just a matter of reducing the microneedle's size though. It will require a serious research effort as the resolution of the fabrication process of the electrode array itself should also be improved upon to yield a similar or better electrode density. Integrating electronics in the implants is also required to achieve much higher channels counts. This is part of our current research effort.

5 Conclusion

Fast resorbing PLGA microneedles are a practical method for inserting ultra-flexible, polyimide-insulated electrode arrays with a wire cross-sectional area of 10 µm². Such implants allow recording of evoked potentials and spontaneous action potentials over chronic timescales, although the latter requires a transition period to stabilize. Only a small lesion remains, which measures about 20% of the cross sectional area of the microneedle. Neurons can be seen to penetrate the area originally taken up by the dissolving PLGA microneedle. Beyond the scar, no drop in neural density was observed. Therefore, the neural implant technology presented forms a reliable foundation for further developments towards high resolution, chronic neural interfacing.

Acknowledgements

Our gratitude goes to Michel Decooman for keeping the cleanroom equipment operational, to Karin Jonckers for helping with the histology, to prof. Erin Koos for kindly providing access to her confocal microscope and to Jean-Paul van Brakel for providing his open-source spike detection algorithm. Research was only made possible by Frederik Ceyssens' research fellowship from FWO-Flanders, the KULeuven IDO fund and further supported by the Hercules Foundation for heavy equipment (AKUL 034 and ZW1115). The research leading to these results has received funding from the European Research Council under the European Union's Seventh Framework Programme (FP7/2007-2013) / ERC grant agreement n° 340931.

Declaration of competing interests

The authors have no competing interests to declare.

REFERENCES

1. A. Berényi, Z. Somogyvári, A.J. Nagy, L. Roux, J.D. Long, S. Fujisawa, E. Stark, A. Leonardo, T.D. Harris, G. Buzsáki, Large-scale, high-density (up to 512 channels) recording of local circuits in behaving animals, Journal of neurophysiology 111 (2013) 1132-1149.
2. A.B. Schwartz, X. T. Cui, D.J. Weber, D.W. Moran, Brain-controlled interfaces: movement restoration with neural prosthetics, Neuron 52 (2006) 205-220.
3. G. Schalk, Brain–computer symbiosis, Journal of neural engineering 5 (2008) 1.
4. J.J. Jun, N.A. Steinmetz, J.H. Siegle, D.J. Denman, M.Bauza, B.Barbarits, A.K. Lee, C.A. Anastassiou, A. Andrei, C. Aydin, M. Barbic, Fully integrated silicon probes for high-density recording of neural activity, Nature 551 (2017) 232.
5. B.C. Raducanu, R.F. Yazicioglu, C.M. Lopez, M. Ballini, J. Putzeys, S. Wang, A. Andrei, M. Welkenhuysen, N. Van Helleputte, S. Musa, R. Puers, Time multiplexed active neural probe with 678 parallel recording sites, In *Solid-State Device Research Conference (ESSDERC), 2016 46th European*, pp. 385-388. IEEE, 2016.
6. V.S. Polikov, P.A. Tresco, W.M. Reichert, Response of brain tissue to chronically implanted neural electrodes, Journal of neuroscience methods 148 (2005) 1-18.
7. A. Wang, X. Liang, I. I. McAllister, P. James, J. Li, K. Brabant, C. Black, P. Finlayson, T. Cao, H. Tang, S.O. Salley, G.W. Auner, Stability of and inflammatory response to silicon coated with a fluoroalkyl self-assembled monolayer in the central nervous system Journal of biomedical materials research Part A 81 (2007) 363-372.
8. H. Hämmerle, K. Kobuch, K. Kohler, W. Nisch, H. Sachs, M. Stelzle, Biostability of micro-photodiode arrays for subretinal implantation, Biomaterials 23 (2002) 797-804.
9. A. Lecomte, E. Descamps, C. Bergaud, A review on mechanical considerations for chronically-implanted neural probes, Journal of neural engineering 15 (2018) 031001.
10. A. Gefen, N. Gefen, Q. Zhu, R. Raghupathi, S.S. Margulies, Age-dependent changes in material properties of the brain and braincase of the rat, Journal of Neurotrauma 20 (2003) 1163-1177.
11. A. Gilletti, J. Muthuswamy, Brain micromotion around implants in the rodent somatosensory cortex, Journal of neural engineering 3 (2006) 189.
12. J. Subbaroyan, D.C. Martin, D.R. Kipke, A finite-element model of the mechanical effects of implantable microelectrodes in the cerebral cortex, Journal of neural engineering 2 (2005) 103.
13. J.K. Nguyen, D. J. Park, J. L. Skousen, A. E. Hess-Dunning, D.J. Tyler, S. J. Rowan, C. Weder, J.R. Capadona, Mechanically-compliant intracortical implants reduce the neuroinflammatory response, Journal of Neural Engineering 11 (2014): 056014.

14. B.A. Wester, R. H. Lee, M. C. LaPlaca, Development and characterization of in vivo flexible electrodes compatible with large tissue displacements, Journal of Neural Engineering 6 (2009) 024002.
15. A. Mercanzini, K. Cheung, D.L. Buhl, M. Boers, A. Maillard, P. Colin, J.C. Bensadoun, A. Bertsch, P. Renaud, Demonstration of cortical recording using novel flexible polymer neural probes, Sensors and Actuators A: Physical 143 (2008) 90-96.
16. J.P. Seymour, D. R. Kipke, Neural probe design for reduced tissue encapsulation in CNS, Biomaterials 28 (2007) 3594-3607.
17. G. Guitchounts, J.E. Markowitz, W.A. Liberti, T. J. Gardner, A carbon-fiber electrode array for long-term neural recording, *Journal of Neural Engineering* 10 (2013) 046016.
18. T. Zhou, G. Hong, T.M. Fu, X. Yang, T. G. Schuhmann, R. D. Viveros, C. M. Lieber, Syringe-injectable mesh electronics integrate seamlessly with minimal chronic immune response in the brain, Proceedings of the National Academy of Sciences 114, no. 23 (2017): 5894-5899.
19. L. Luan, X. Wei, Z. Zhao, J.J. Siegel, O. Potnis, C.A. Tuppen, S.Lin, S. Kazmi, R.A. Fowler, S. Holloway, A.K. Dunn, Ultraflexible nanoelectronic probes form reliable, glial scar–free neural integration, Science advances 3 (2017) e1601966.
20. X. Jiao, Y. Wang, Q. Qing, Scalable fabrication framework of implantable ultrathin and flexible probes with biodegradable sacrificial layers, Nano letters 17 (2017) 7315-7322.
21. C. Xie, J. Liu, T.M. Fu, X. Dai, W. Zhou, C.M. Lieber, Three-dimensional macroporous nanoelectronic networks as minimally invasive brain probes, Nature materials 14, (2015) 1286.
22. T.D.Y. Kozai, Z. Gugel, X. Li, P.J. Gilgunn, R. Khilwani, O. B. Ozdoganlar, G.K. Fedder, D.J. Weber, X.T. Cui, Chronic tissue response to carboxymethyl cellulose based dissolvable insertion needle for ultra-small neural probes, Biomaterials 35 (2014) 9255-9268.
23. J. Agorelius, F. Tsanakalis, A. Friberg, P.T. Thorbergsson, L.M.E. Pettersson, J. Schouenborg, An array of highly flexible electrodes with a tailored configuration locked by gelatin during implantation—initial evaluation in cortex cerebri of awake rats, Frontiers in neuroscience 9 (2015) 331.
24. A. Lecomte, V. Castagnola, E. Descamps, L. Dahan, M. C. Blatché, T. M. Dinis, E. Leclerc, C. Egles, C. Bergaud, Silk and PEG as means to stiffen a Parylene probe for insertion in the brain: toward a double time-scale tool for local drug delivery, Journal of Micromechanics and Microengineering 25 (2015) 125003.
25. A. Lecomte, A. Degache, E. Descamps, L. Dahan, C. Bergaud, In vitro and in vivo biostability assessment of chronically-implanted Parylene C neural sensors, Sensors and Actuators B: Chemical 251 (2017) 1001-1008.
26. Z. Xiang, S.C. Yen, N. Xue, T. Sun, W. M. Tsang, S. Zhang, L.D. Liao, N. V. Thakor, C. Lee, Ultra-thin flexible polyimide neural probe embedded in a dissolvable maltose-coated microneedle, Journal of Micromechanics and Microengineering 24 (2014) 065015.
27. D. Lewitus, K.L. Smith, W. Shain, J. Kohn, Ultrafast resorbing polymers for use as carriers for cortical neural probes, Acta biomaterialia 7 (2011) 2483-2491.
28. J.Paul (2018) https://stackoverflow.com/questions/22583391. Accessed 30/3/2018.
29. J.N. Turner, W. Shain, D. H. Szarowski, M. Andersen, S. Martins, M. Isaacson, H. Craighead, Cerebral astrocyte response to micromachined silicon implants. Experimental neurology 156 (1999) 33-49.
30. M.I. Sabir, X. Xu, L. Li, A review on biodegradable polymeric materials for bone tissue engineering applications, Journal of materials science 44 (2009) 5713-5724.
31. F. Ceyssens, R. Puers, Insulation lifetime improvement of polyimide thin film neural implants, Journal of Neural Engineering 12 (2015) 054001.
32. N. Lago, K. Yoshida, K. P. Koch, X. Navarro, Assessment of biocompatibility of chronically implanted polyimide and platinum intrafascicular electrodes, IEEE Transactions on Biomedical Engineering 54, (2007) 281-290.
33. J.M. Seo, S.J. Kim, H. Chung, E.T. Kim, H.G. Yu, Y.S. Yu, Biocompatibility of polyimide microelectrode array for retinal stimulation, Materials Science and Engineering: C 24 (2004) 185-189.
34. R. Richardson Jr, J. A. Miller,W.M. Reichert, Polyimides as biomaterials: preliminary biocompatibility testing, Biomaterials 14 (1993) 627-635.
35. B. Wessling, W. Mokwa, U. Schnakenberg, RF-sputtering of iridium oxide to be used as stimulation material in functional medical implants, Journal of Micromechanics and Microengineering 16 (2006) S142.
36. Z.J. Chen, G. T. Gillies, W.C. Broaddus, S.S. Prabhu, H. Fillmore, R.M. Mitchell, F.D. Corwin, P.P. Fatouros, A realistic brain tissue phantom for intraparenchymal infusion studies, Journal of Neurosurgery 101 (2004) 314-322.
37. Z.J. Du, C.L. Kolarcik, T.D. Kozai, S.D. Luebben, S.A. Sapp, X.S. Zheng, J.A. Nabity, X.T. Cui, Ultrasoft microwire neural electrodes improve chronic tissue integration, Acta biomaterialia 53 (2017) 46-58.
38. G. Buzsáki, C.A. Anastassiou, C. Koch, The origin of extracellular fields and currents—EEG, ECoG, LFP and spikes, Nature Reviews Neuroscience 13(2012) 407.
39. H. Lütcke, D.J. Margolis, F. Helmchen, Steady or changing? Long-term monitoring of neuronal population activity, Trends in Neurosciences 36 (2013) 375-284.
40. R. Khilwani, P.J. Gilgunn, T.D.Y. Kozai, X. C. Ong, E. Korkmaz, P.K. Gunalan, X. T. Cui, G.K. Fedder, O. B. Ozdoganlar, Ultra-miniature ultra-compliant neural probes with dissolvable delivery needles: design, fabrication and characterization, Biomedical Microdevices 18 (2016) 97.
41. A. Mercanzini, K. Cheung, D. Buhl, M. Boers, A. Maillard, P. Colin, J.C. Bensadoun, A. Bertsch, A. Carleton, P. Renaud, Demonstration of cortical recording and reduced inflammatory response using flexible polymer neural probes. In IEEE 20th International Conference on Micro Electro Mechanical Systems(MEMS) (2007) 573-576.
42. A. Altuna, J. Berganzo, L.J. Fernández, Polymer SU-8-based microprobes for neural recording and drug delivery. Frontiers in Materials 2 (2015) 47.

Supplementary material: detailed methods

1. PLGA microneedle fabrication

PLGA needles were fabricated using a laser micromachining process. First, PLGA sheets were made out of Corbion Purasorb PLDG 5002A, an acid-terminated human-rated type of PLGA with a 50-50 lactic and glycolic acid ratio. Pellets of the material, which melt around 90°C, were put on a Teflon FEP 125 foil and melted on a hotplate. They were heated to 180 °C to reduce viscosity and facilitate degassing. Then, the melt was cooled down to 120 °C to increase viscosity and sheets of 100 and 200 µm thickness were fabricated using doctor blading. Afterwards, the foil was taken off the hotplate immediately.

Laser milling was performed using an Oxford Lasers J picosecond laser milling station using a 4W 20 µJ/pulse Talisker Ultra 355-4 mode-locked fiber seed laser with a diode-pumped solid-state amplifier, operating at a 355 nm wavelength. A PLGA sheet was suspended one mm above a silicon substrate in order to avoid ablating the substrate, with subsequent re-deposition of material on the PLGA. The laser was set to circumscribe the needle shape 5 times with each line 7 micrometers apart. Laser power was set at 55%, write speed at 600 mm/s and downward step was 5 micron. Laser writing was interrupted manually when the structures were seen to come loose, which was typically after 25 steps.

2. Non-resorbable electrode array fabrication

On 4 inch silicon carrier wafers, a 100 nm thick aluminum sacrificial layer was deposited using thermal evaporation. PI 2611 polyimide, diluted in NMP 1:1 by weight, was spin coated at 2000 rpm and baked 90 seconds at 90°C and 90 seconds at 150°C on a hotplate to yield a layer thickness of 500 nm. Thereafter, it was baked in a convection oven for 1 hour at 200°C. Temperature was ramped up and down at 4 degrees per minute, starting and ending at room temperature. A two layer liftoff resist layer was then deposited (LOR10B, spin coated at 3500 rpm for 30 seconds, baked at 180°C for 5 minutes on a hotplate, then S1818 positive photoresist spin coated at 4000 rpm and baked at 100°C for 2 minutes). The resist layer was patterned lithographically (broadband UV exposure at 25 mJ/cm², then development in 4:1 diluted 351 developer for 2'30" lying horizontally in a beaker). A 80 nm thick Pt layer was sputtered in a BAE370 sputter coater with 3 inch targets, followed by a 110 nm thick sputtered iridium oxide layer on top to reduce electrode impedance [35]. Sputtering parameters were: $2*10^{-3}$ mbar pressure, 70 sccm Ar flow with 5 sccm O_2 flow added during iridium oxide sputtering. To reduce thermal load, sputtering was done with the wafers held on a rotating table, exposing them to the plasma only $1/9^{th}$ of the sputtering time. Sputtering time was 19 minutes for Pt and 18 minutes for Irox. Between Pt and Irox sputtering, the vacuum was broken to install a shadow mask, that precluded sputtering of Irox on the bondpads of the devices. After sputtering, the wafers were put in NMP overnight to dissolve the liftoff resist. A water rinse completes metal patterning.

Then, a second PI2611 polyimide layer (also diluted 1:1 by weight in NMP) was then spun on at 2600 rpm, baked 90 seconds at 90°C and 90 seconds at 150°C on a hotplate and then baked in a convection oven under nitrogen atmosphere. Oven temperature was ramped up to 350°C, with a ramp rate of 4 °C/min until 200°C, then a pause of 30 minutes and a ramp of 2.5°C/min afterwards. Ramping down was also done at 2.5°C/min. Then, an 100 nm thick aluminum hard mask was deposited using thermal evaporation, and patterned lithographically (S1818 photoresist spin coated at 3000 rpm, baked 2 minutes at 100°C, exposed at 40 mJ/cm², developed 1' in 3:1 diluted 351 developer). Then reactive ion etching (RIE) was used to pattern the polyimide and open up the electrodes and bond pads. Etching parameters were: 30 mTorr pressure, 20 sccm O_2 flow, 5 sccm SF6 flow, 150W RF power (13.56 MHz), 2'15" etch time). The photoresist was then stripped (aceton+IPA dip) and the aluminium hard mask removed by dipping in 5 wt% HCl.

The impedance spectrum of that electrodes in phosphate buffered saline was tested using a MultiChannel Systems NanoZ device. For allowing these tests on a released device, we fabricated a thicker, self-supporting version as well.

The wafer was diced. An 18-pin Omnetics Nano connector was soldered to the bondpads and EpoTek H54 epoxy was applied as underfill below the connector. The epoxy was baked at 150 °C for one hour.

3. Microneelde – electrode array bonding

To embed the electrode array, a 100 µm thick microneedle was positioned on top using fine tweezers under a stereomicroscope and was then attached by a short heating step (1 minute at 75°C) on a hotplate. The assembly was then released from the wafer by immersing in 5% HCl, dissolving the aluminum sacrificial layer. A second microneedle was then attached to the bottom in a similar way, while the assembly was resting on a Teflon FEP sheet to prevent stiction.

4. In vivo tests

3.1 Regulations and housing

The research project was executed in accordance with the Belgian and European laws, guidelines and policies for animal experimentation, housing and care (Belgian Royal Decree of 29 May and European Directive 2010/63/EU on the protection of animals used for scientific purposes of 20 October 2010). The animal experiments were performed on four male Wistar rats, weighing about 250 g on arrival. The animals were housed and maintained in standard cages under conventional laboratory conditions with *ad libitum* access to food and water and a 12 h light/12 h dark cycle. The experiments were conducted during the light phase of the animals' activity cycle. Two additional rats were used for a pilot study in which only the PLGA needles were implanted, without electrode array.

3.2 Implantation procedure

The rats were anesthetized using an isoflurane/oxygen pump system (Iso-vet Surgivet at 3% for induction and 1–2% maintenance; O2 1 L/min) and then placed in the stereotactic frame (Stoelting Co) with constant isoflurane/oxygen delivered through a face mask. The hair above the area of surgery was epilated and the skin opened with a blade after the application of additional subcutaneous anesthetics (Xylocaine 2%, 1:200,000 adrenaline, AstraZeneca). A hole was drilled 4 mm right from bregma, over the sensorimotor cortex. The

implants were desinfected using 70% isopropanol for 5 minutes, air dried and then inserted in the hole to a depth of 3 mm with the help of metal stereotactic adaptors. The implant was then fixed to the skull with UV-cured dental cement (Tetric EvoFlow, Ivoclar Vivadent). Afterwards, the connector was also fixed on the skull with the support of stainless steel inserted screws, together with the reference electrode that was wrapped around one of the screws. When everything was sealed with the dental cement, the wound was sutured. Pain relief was ensured for 24 h with 0.06 mg/kg Vetergesic (Ecu phar).

3.3 Electrical measurements

To test the recording capabilities of the implanted electrode array in the rat brain, controlled electrical stimulation was selected as a measurement strategy. The rats were anesthetized as described above and put in a Faraday cage. Since the recordings took place in the right somatosensory cortex, the contralateral (left) paw of the anesthetized rat was stimulated. A 26G hypodermic needle was inserted subcutaneously to the back of the front left paw and connected to a stimulus generator (Multichannel systems, STG2004). An anal probe was used as counter electrode. The implant was connected to a data acquisition system (Multichannel Systems USB-ME32-FAI-System) and recording was started. First, the spontaneous neural activity was recorded for 4 minutes. Finally, in order to provoke an evoked potential, an electrical stimulus (biphasic, 0.8 mA, 1 ms per phase, 10 s interval) which clearly produced local muscle contractions was applied to the left forepaw.

The impedance of the electrodes with respect to the reference electrode situated in the skull was also determined before, 2 and 4 months after implantation at a frequency of 1004 Hz, using a Multichannel Systems NanoZ impedance recording device.

3.4 Data processing of electrical measurements

As the evoked response is at relatively low frequencies, the measured signals were high-pass filtered using a finite impulse response (FIR) filter with a stop band below 10 Hz and a 40 dB minimum attenuation in the stop band. A Matlab script was written to determine the stimulation artifact position based on a threshold value and its repetition period. The script allowed to check the results manually and to adapt the threshold if required. Then, the peak-to-peak (PTP) values of the evoked potential in the brain were determined, as well as its root mean square (RMS) value, in absolute terms as well as relative with respect to the period before the stimulation artifact. For the latter the RMS value of the window 650 ms after the stimulation pulse was divided by the RMS value in the 150 ms window before the pulse.

For quantifying spikes in the measured spontaneous neural activity, the data were high pass filtered using a FIR high-pass filter with 40 dB attenuation, a 200 Hz stop band and a 250 Hz pass band. An open-source peak-detection algorithm based on a moving average and standard deviation [28] with a time window of 200 samples was used. A spike was defined as a negative signal deviating more than 4 times the moving standard deviation of the signal from the moving average.

3.5 Perfusion

At the end of the experiments, the animals were given a lethal dose of pentobarbital and perfused intracardially using 250 ml of phosphate-buffered saline (PBS) and then 200 ml of 4% paraformaldehyde (PFA). The brains were extracted and kept in 4% PFA for 24 hours. Then, they were rinsed in PBS overnight and later kept in 20% sucrose and 0.1% sodium azide in PBS until slicing was done.

For the slicing procedure, the samples were embedded in 4% agar gel. The vibrotome (Leica VT1000S) was set at a cutting thickness of 125 µm. Slices were made top-down in the transversal plane.

3.6 Histology

Slices were stained with a NeuN (for highlighting Neuron Neuclei) and GFAP (for showing astrocytes) double immunostain as follows: they were put overnight in blocking buffer (1% BSA, 0.1% Triton X100 in PBS). Then, primary antibodies were applied (1:100 MAB377 mouse anti-NeuN, 1:500 polyclonal rabbit anti-GFAP Z0334 in blocking buffer) overnight at room temperature while shaking very mildly. The samples were washed 3 times in PBS for 10 minutes. Then, they were incubated in blocking buffer for 2 hours at room temperature. Then, secondary antibodies were applied (Alexa Fluor 488 donkey anti mouse IgG (H+L) and Cy3 Donkey Anti Rabbit IgG (H+L), 1:1000 in blocking buffer). Finally, the slices were washed 3 times in PBS again for 10' and then mounted embedded in Sigma Fluoroshield on Superfrost microscope glasses. Slices were imaged using a Leica TCS SP8 confocal microscope using a 20x immersion objective. The main imaging parameters were: 1024x1024 pixel imaging, 5% 488 nm laser power, 3% 552 nm laser power, Cy3 and Alexa 488 filters and 950 and 830 amplifier gain, respectively.

For the pilot study on PLGA needles without an electrode array, the boundary of the scar in the GFAP images (which showed a clear inner border) was outlined manually in the ImageJ software package (v1.51n) and the surface of the scar was calculated. The area without viable neurons (as seen on NeuN stain) was determined similarly. For the experiment with electrodes, this procedure was followed as well. Furthermore, the neuron density was determined in and between circles of 350, 600 and 1000 µm diameter around the implant center. For this, the background of the NeuN stained was first reduced using ImageJ's 'Remove Background' function. Contrast was enhanced using the 'Enhance Contrast' function of the Gimp (v2.8) software package with a threshold of 50%. Then two manual counts were done and the results averaged.
